Turbulence, Heat and Mass Transfer 4
K. Hanjalic, Y. Nagano and M. Tummers (Editors)
©2003 Begell House, Inc.

The Role of Splatting Effect in High Schmidt Number Turbulent Mass Transfer Across an Air-Water Interface

Y. Hasegawa and N. Kasagi
Department of Mechanical Engineering, The University of Tokyo, Hongo, Bunkyo-ku, Tokyo 113-8656, Japan

Abstract- High Schmidt number gas absorption into liquid across an air-water interface is simulated by means of a hybrid DNS/LES scheme. The results are well compared with those previously obtained by a Lagrangian method. Due to the wind shear, quasi-streamwise vortices are generated beneath the interface. They induce upwelling flows which impinge on the interface, *i.e.*, splatting. At high Schmidt numbers, the concentration field near the interface is characterized by low concentration spots, which occur intermittently associated with the splatting events, and fine-scale high concentration streaks produced by the interfacial shear. With an assumption that the surface renewal period should be equal to the typical time scale of the quasi-streamwise vortex, the gas transfer rate is well predicted. Therefore, it is the quasi-streamwise vortex scaled by the shear units that governs the mass transfer across a shear-driven air-water interface.

1. Introduction

Gas exchange across the sea surface plays a crucial role in the global carbon cycle on the earth, and better understanding of the mechanism controlling the interfacial mass transfer is indispensable to improve the model prediction of the global air-sea CO_2 fluxes. For slightly soluble gases such as carbon dioxide, most mass transfer resistance occurs in liquid. Additionally, with the Schmidt number of about 1000, the transport process is governed by near-surface turbulence within a thin concentration boundary layer (20 ~ 200 μm). Since the simultaneous measurement of the velocity and scalar fields is extremely difficult in experiments, the mechanism of the mass transfer is not understood well.

When predicting the gas transfer rate K, the time scale of vortices which govern the mass transfer has been a subject of discussion. For instance, if one selects the time scale of the large eddies scaled by l / u^*, one obtains $K \propto Sc^{-1/2} Re_*^{-1/2}$, while $K \propto Sc^{-1/2} Re_*^{-1/4}$ by assuming the transfer is governed by the small eddies responsible for the dissipation. Here, $Re_* = u^* l / \nu$ and l is the integral length scale. In the last decade, direct numerical simulation (DNS) has been applied to free-surface flows by several groups [1-3], and the complex interaction between a free surface and turbulent structures, and the associated transport process have been studied. However, since the number of grid points for resolving the scalar field increases in proportion to $Sc^{3/2}$, the Schmidt number of scalar has been limited to $Sc \sim O(1)$ in most of the previous calculations.

In this study, DNS of a coupled air-water turbulent flow is carried out in order to investigate the structures of the scalar field and microscopic mechanism of the mass transfer near the interface. A hybrid DNS/LES scheme, in which DNS is applied in a near-surface region by concentrating grids, while LES in the outer region with relatively coarse grids, is proposed to calculate the scalar field at the high Schmidt number of $Sc_L = 100$. The obtained gas transfer rate is well compared with the Lagrangian result and the detailed mass transfer mechanism is discussed.

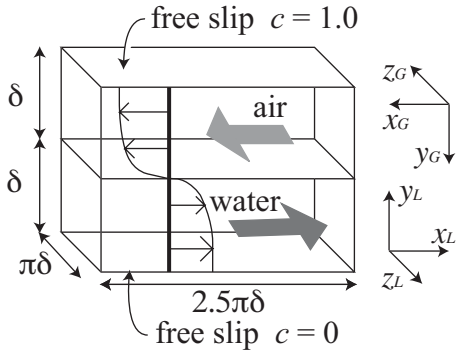

Fig. 1: Computational domain and coordinate system

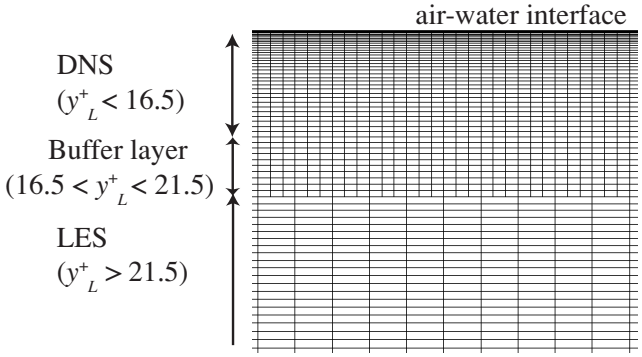

Fig. 2: Grid system for solving scalar field with hybrid DNS / LES scheme

2. Numerical Methodology

2. 1 Computational Condition

A fully developed air-water counter flow driven by a constant pressure gradient and the associated interfacial mass transfer are considered as shown in Fig. 1. The governing equations in the two phases are the incompressible Navier-Stokes, continuity, and scalar transport equations, *i.e.*,

$$\frac{\partial u_i}{\partial t} + u_j \frac{\partial u_i}{\partial x_j} = -\frac{\partial p}{\partial x_i} + \frac{1}{Re_\tau} \frac{\partial^2 u_i}{\partial x_j \partial x_j}, \qquad \frac{\partial u_i}{\partial x_i} = 0, \tag{1}$$

$$\frac{\partial c}{\partial t} + u_j \frac{\partial c}{\partial x_j} = \frac{1}{Sc \cdot Re_\tau} \frac{\partial^2 c}{\partial x_j \partial x_j}, \tag{2}$$

where u_i is i-th velocity component, x_i the coordinates, c the scalar concentration. Subscripts 1, 2, and 3 correspond to streamwise, vertical and spanwise directions, respectively. All variables are normalized by the friction velocity u_τ and the depth δ in each phase. The Reynolds number and the Schmidt number are defined as $Re_\tau = u_\tau \, \delta / \nu$ and $Sc = \nu / D$, where ν and D are the kinematic viscosity and the molecular diffusivity of scalar, respectively. In this study, the Reynolds numbers in the two phases are set to be $Re_{\tau L} = Re_{\tau G} = 150$, which corresponds to the air-water flow at the wind velocity of 2 m/s and the phase depth of 4 cm under the standard condition. The Schmidt number is changed from 1.0 to 100 in liquid, while kept constant $Sc_G = 1.0$ in gas. Since it is known that the interfacial deformation is negligibly small in the low Reynolds number flow considered here, the interface is assumed to be flat. Therefore, the resultant boundary conditions at the interface are the continuity of the horizontal velocities and shear stress for the velocity field, and the Henry's law and the continuity of the scalar flux for the scalar field. They are given as:

$$u_{2L} = u_{2G} = 0, \tag{3}$$

$$u_{iL} = R_\rho \cdot u_{iG}, \qquad \frac{\partial u_{iL}}{\partial x_{2L}} = R_\nu \cdot \frac{\partial u_{iG}}{\partial x_{2G}}, \quad (i = 1, 3) \tag{4}$$

$$c_L = \alpha \cdot c_G, \qquad \frac{\partial c_L}{\partial x_{2L}} = R_\rho \cdot R_\nu \cdot \frac{Sc_L}{Sc_G} \cdot \frac{\partial c_G}{\partial x_{2G}}. \tag{5}$$

Here, α is dimensionless Ostwald's solubility. The two non-dimensional parameters of R_ρ and

Table. 1: Number of modes k_x, k_z and grid points N_y, and their spacing Δx^+, Δy^+ and Δz^+ for three regions in hybrid DNS/ LES scheme.

	Region	k_x , N_y , k_z	Δx_L^+	Δy_L^+	Δz_L^+
DNS	$0 < y_L^+ < 16.5$	512, 95, 512	2.3	0.002 ~ 0.34	0.9
Buffer	$16.5 < y_L^+ < 21.6$	512, 14, 512	2.3	0.35 ~ 0.38	0.9
LES	$21.6 < y_L^+ < 150$	64, 324, 64	18.4	0.002 ~ 0.38	7.2

R_ν in Eqs. (4) and (5) represent a degree of dynamical coupling between the two fluids, and are defined as:

$$R_\rho = \sqrt{\rho_L / \rho_G}, \quad R_\nu = (\nu_G / \nu_L) \cdot R_\rho^{-1}. \tag{6}$$

In this study, R_ρ and R_ν are set to be 29 and 1.0, respectively. At the outer boundaries, a free-slip condition is imposed for the velocity field in order to minimize the effect of the assumed outer boundary condition, and a constant concentration condition for the scalar fields, *i.e.*, c = 1.0 and 0 at the top and bottom boundaries, respectively.

2. 2 Numerical Scheme

A pseudo-spectral method with Fourier expansions in the x and z directions and Chebyshev polynomials in the y direction, is employed for spatial discretization of the velocity and scalar fields at Sc_L = 1.0, 3.0 and 5.0. The numbers of modes employed for the velocity field in the three directions are (k_x , k_y , k_z) = (64, 288, 64) and their spacings are (Δx^+ , Δy^+ , Δz^+) = (18.4, 0.0045 ~ 0.82, 7.2). Time advancement is made by the second-order Adams-Bashforth method for the convective terms and the Crank-Nicolson method for the diffusion terms. The details of the numerical algorithm employed are essentially the same as those of Lombardi *et al*. [1].

2. 2. 1. Hybrid DNS / LES scheme

In order to calculate the concentration filed at the Schmidt number of Sc_L = 100, we propose a hybrid DNS / LES scheme in which DNS with high-resolution grids is applied within the near-interface region, while LES with coarser grids for the outer layer (see, Fig. 2). For spatial discretization, Fourier expansions are used in the x and z directions, while the second-order finite difference scheme is employed in the y direction in order to avoid complexity of numerical procedures. The computational domain in liquid is divided into three regions, *i.e.*, DNS region ($0 < y^+_L < 16.8$), buffer region ($16.8 < y^+_L < 21.5$), and LES region ($y^+_L > 21.5$). The numbers of modes and grid points employed in each region are listed in Table. 1.

Since the finer grid system is employed for the scalar field in the DNS region, the fluid velocities should be appropriately interpolated in order to evaluate the convective terms accurately. In this study, the Fourier-Chebyshev interpolation scheme, in which fast Fourier and Chebyshev transforms are used by setting the components of higher wave numbers to be zero, is employed.

In the outer layer, the same grid system as that of the velocity field is employed. Since the grids are not fine enough to resolve the scalar dissipation, the constant Smagorinsky model is introduced in order to dissipate the scalar fluctuation appropriately. This results in:

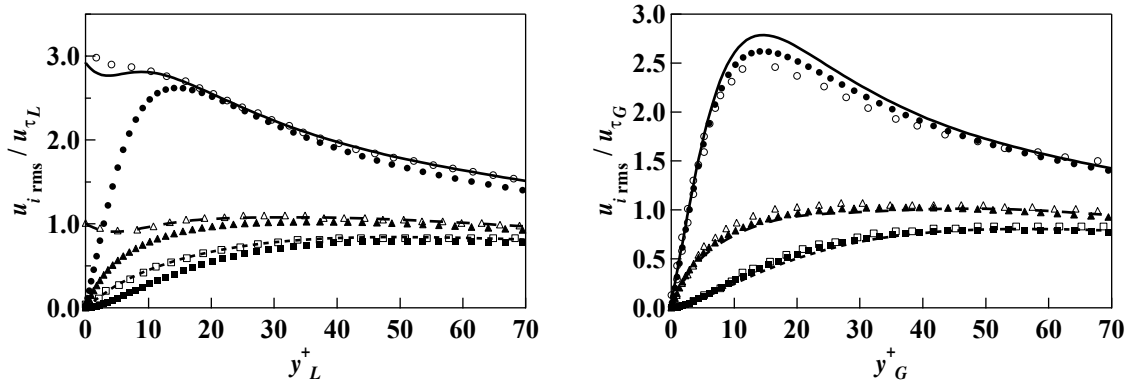

Fig. 3: Velocity fluctuations in a) liquid and b) gas. Present study; ——: u_{rms}, - - -: v_{rms}, — -: w_{rms}, Lombardi *et al.*; ○: u_{rms}, □: v_{rms}, △: w_{rms}, Channel; ●: u_{rms}, ■: v_{rms}, ▲: w_{rms} .

$$\frac{\partial c}{\partial t} + u_j \frac{\partial c}{\partial x_j} = \frac{1}{Sc \cdot Re_\tau} \frac{\partial^2 c}{\partial x_j \partial x_j} + \frac{\partial \xi_j}{\partial x_j}, \tag{7}$$

$$\xi_j = -D_s \Delta^2 \left| S_{ij} \right| \frac{\partial c}{\partial x_j}, \qquad \Delta = (\Delta x \cdot \Delta z)^{1/2}. \tag{8}$$

The model coefficient D_s is determined by the previous *a priori* test data for a low Schmidt number, since it was found that the model coefficient is almost independent of the Schmidt number near the interface [5]. It is possible to use more complex models such as dynamic Smagorinsky model or mixed model to improve the model prediction. It should be noted, however, that most change of the mean concentration occurs in the DNS region (see, Fig. 4) and therefore, the effect of the SGS model on the total scalar transfer is insignificant.

As is well known, employment of a hybrid scheme such as detached eddy simulation, frequently leads to a mismatch of the mean profile at the connection point between two schemes. In order to avoid this, we establish a buffer region between the two regions, where the SGS model is gradually imposed as going away from the interface by increasing the Smagorinsky constant.

2. 2. 2. Lagrangian method

We also applied a Lagrangian method to the mass transfer at the high Schmidt numbers from 100 to 1000. In this method, the concentration field is represented by the probability density function of a large number of scalar markers, which move due to the convective and molecular effects. The details of the numerical scheme can be found in Papavassiliou and Hanratty [4].

3. Results

3. 1 Velocity field

The velocity fluctuations in gas and liquid are shown in Fig. 3 as a function of the distance from the interface. In liquid, the horizontal velocity fluctuations $u_{L\,rms}$ and $w_{L\,rms}$ have peaks at their interface, while those in gas are decreased with approaching the interface. These differences result from a high density ratio R_ρ of the two fluids in Eq. (4). Hence, the interface is similar to a solid wall for gas, while a free surface for liquid. However, coherent structures scaled by the shear units, such as low and high speed streaks and quasi-streamwise vortices, are observed in both phases despite the difference in the effects of the boundary. Since the present paper focuses on the scalar field, the statistics of the velocity fields are referred to the previous work [1].

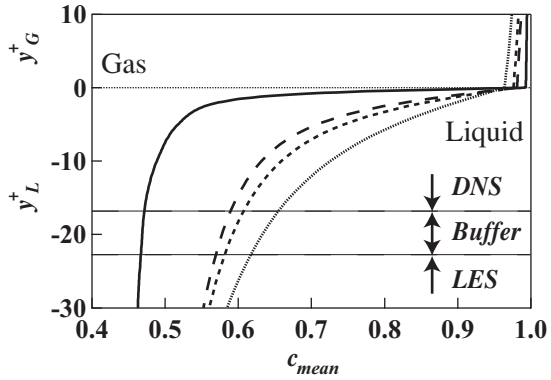

Fig. 4: Mean concentration profiles. ..... : $Sc_L = 1.0$, - - -: $Sc_L = 3.0$, — —: $Sc_L = 5.0$, ——: $Sc_L = 100$.

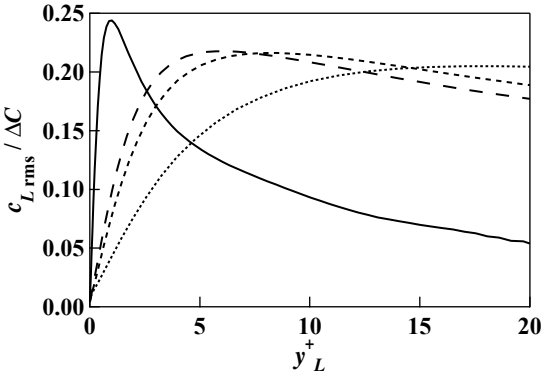

Fig. 5: Concentration fluctuation profiles in liquid. For symbols see Fig. 4.

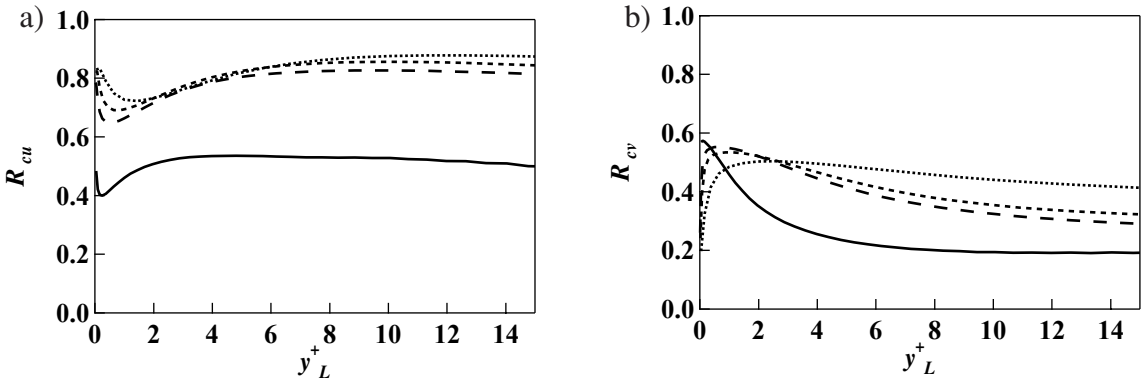

Fig. 6: Correlation coefficient a) R_{cu} and b) R_{cv}. For symbols see Fig. 4.

3. 2 Scalar field

3. 2. 1. Eulerian analysis

The mean concentration profiles for different Schmidt numbers near the interface are shown in Fig. 4. In all cases, the change of the mean concentration mainly occurs in the liquid phase, and the thickness of the concentration boundary layer rapidly decreases with increasing the Schmidt number. At Sc_L = 100, more than 95% of the mean concentration change occurs in the DNS region ($y^+_L < 16.8$), and a smooth profile without a mismatch at the connection between the DNS and LES regions is obtained by the hybrid scheme. In Fig. 5, the concentration fluctuations in liquid are shown. Although the location of the peak approaches the interface in inverse proportion to $Sc_L^{1/2}$, the concentration fluctuation outside the DNS region is not negligible even at Sc_L = 100, which indicates the importance of coupling between the concentration fields in the DNS and LES regions.

In Fig. 6 a) and b), the correlation coefficients R_{cu}, R_{cv} between the concentration c and the streamwise and normal velocities u, v are shown. Although the concentration field at higher Schmidt numbers is less analogous to the velocity field far from the interface, the correlation coefficient between the concentration and normal velocity R_{cv} is kept high around 0.6 near the interface. This suggests that the scalar fluctuation responds to the normal velocity fluctuation quickly even at high Schmidt numbers. This tendency presents a striking contrast to that of R_{cv} near a solid wall [6], in which the scalar fluctuations at higher wave numbers are more damped and the analogy between momentum and mass transfer breaks down. In Fig. 7 a) and b), instan-

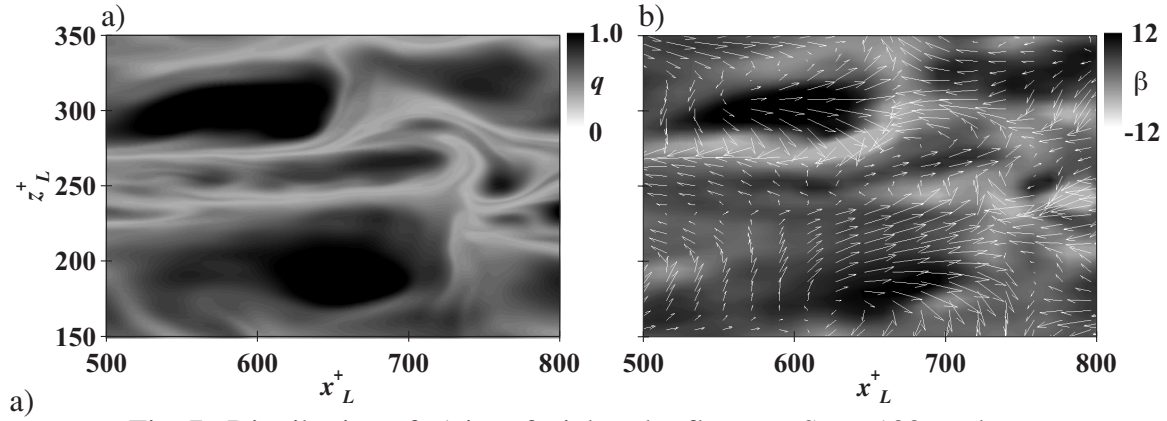

Fig. 7: Distribution of a) interfacial scalar flux q at $Sc_L = 100$, and b) surface divergence β and the velocity vectors.

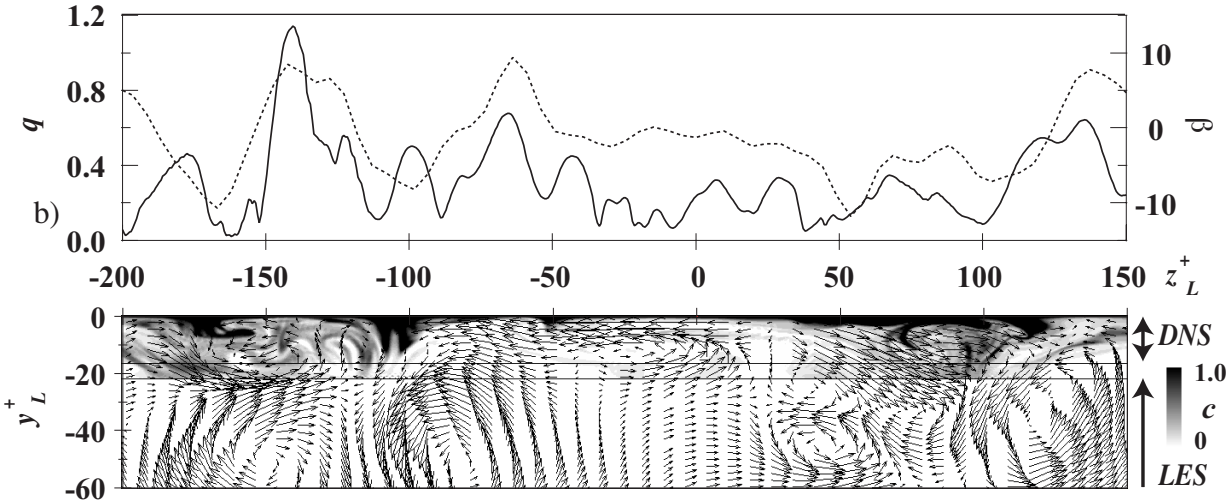

Fig. 8: a) Profiles of interfacial scalar flux q at $Sc_L = 100$: ——, and surface divergence β: ……, b) Instantaneous scalar field at $Sc_L = 100$, and velocity vectors in y-z plane.

taneous distributions of the interfacial scalar flux q at $Sc_L = 100$ and the surface divergence β are shown. The surface divergence can be interpreted as a degree of replacement of the fluids near the interface with those beneath the interface, *i.e.*, surface renewal, which is defined as:

$$\beta = \frac{\partial u}{\partial x} + \left.\frac{\partial w}{\partial z}\right|_{int\,erface} = -\left.\frac{\partial v}{\partial y}\right|_{int\,erface}. \qquad (9)$$

In Fig. 7 a), fine-scale streaky structures and large spotty structures with low and high interfacial scalar flux q, are observed. The spotty high scalar flux regions coincide with high surface divergence regions in Fig. 7 b), where the low concentration fluid impinges to the interface. These spotty structures are observed in both low and high Schmidt numbers, and result in high correlation R_{cv} near the interface (see Fig. 6 b)).

In Fig. 8 a) and b), distributions of the interfacial scalar flux q and the surface divergence β along the z direction, and the simultaneous velocity and scalar fields in the y-z plane are shown. The spatial distribution of the interfacial scalar flux exhibits sharp changes, which correspond to the fine-scale streaky structures with low interfacial scalar flux observed in Fig. 7 a). On the other hand, the striking peaks coincide with the high surface divergence regions caused by upwelling flows associated with quasi-streamwise vortices, *i.e.*, splatting. This indicates that the

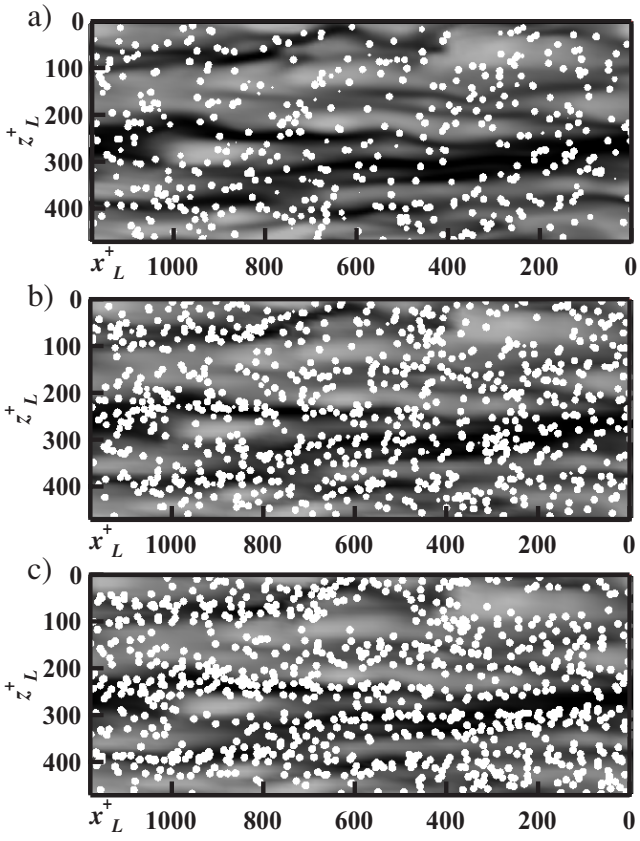

Fig. 9: Distributions of scalar markers near the interface in liquid.
a) Sc_L = 0.1, b) Sc_L = 1.0, c) Sc_L = 100.

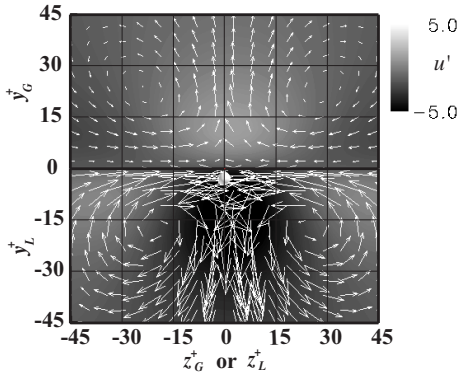

Fig. 10: LSE velocity field around a marker (Sc_L = 100) which passes downward the plane of y^+_L = 3.

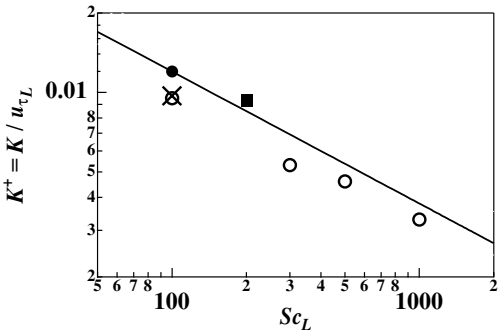

Fig. 11: Gas transfer rates at high Sc_L. present study; ×:Eulerian, ○: Lagrangian, ——: Hanratty, ●: De Angelis *et al.*, ■: Calmet and Magnaudet.

splatting penetrates the concentration boundary layer and enhances the interfacial mass transfer.

3. 2. 2. Lagrangian analysis

In the Lagrangian method, 128 x 128 scalar makers are uniformly disposed at the interface as an initial condition and the time development of the probability density functions of the makers was calculated to investigate the mechanism of scalar transfer from the interface to the bulk in liquid. In Fig. 9, the distributions of the scalar markers at different Schmidt numbers near the interface (y^+_L < 3) at t^+_L = 100 after release are shown. Since the convective effect governs the movement of the scalar makers at high Schmidt numbers, the markers nearly follow the fluid particles and cluster around low speed streaks where the surface divergence is negative (see, Fig. 9 c)). On the other hand, spotty regions with few particles, caused by up-current of the high speed fluid beneath the interface, are also observed. These results are consistent with those obtained by the hybrid scheme, in which the concentration field near the interface is characterized by the low concentration spots caused by splatting, and the high concentration streaks.

In Fig. 10, the typical velocity field around a scalar maker which passes downward y^+_L = 3 plane at Sc_L = 100 is obtained by linear stochastic estimation. It is observed that quasi-streamwise vortices cause the strong downward motion near the interface and enhance the mass transfer.

3. 2. 3. Gas transfer rate

Finally, the gas transfer rates at high Schmidt numbers obtained by the hybrid DNS/LES scheme

and the Lagrangian method are compared in Fig. 11. The previous experimental data obtained by Hanratty [7], and the numerical data by De Angelis *et al.* [3] and Calmet and Magnaudet [8] are also plotted. The gas transfer rates $K^+ = K / u_{\tau L}$ at $Sc_L = 100$ obtained by the hybrid and Lagrangian methods are 0.0097 and 0.0095, respectively, and show very good agreement. If we assume that the time scale of the quasi-streamwise vortex should be equal to $\pi l_v / u_{\tau L}$, where $l_v^+ = 35$ is the diameter of the vortex estimated from the spanwise two point correlation of the normal velocity v (see, also Fig. 10), $K^+ = 0.095\, Sc_L^{-1/2}$ is obtained by using the surface renewal theory. The quantitative agreement between our results and the model prediction indicates that the surface renewal is governed by the quasi-streamwise vortices in liquid. The gas transfer rate is inversely proportional to $Sc_L^{1/2}$, and the qualitative agreement between the present and previous data is fairly good. The underestimation in the present study is mainly due to the low Reynolds number flow considered here, since the normal velocity fluctuation near the interface, *i.e.*, splatting, is enhanced with increasing the Reynolds number. At high Reynolds numbers, the effect of capillary waves should be also taken into account. It will be studied in our future work.

4. Conclusions

High Schmidt number gas absorption into liquid across an air-water interface was successfully calculated by the hybrid DNS/LES scheme, suggesting that it is a promising tool for analyzing multiple-scale heat and mass transfer phenomena. Due to the wind shear, coherent turbulent structures are generated in liquid, and quasi-streamwise vortices induce impingement of upwelling flows on the interface, *i.e.*, splatting. The splatting motion causes intermittent low concentration spots near the interface and enhances the interfacial scalar flux by replacing the fluids adjacent to the interface with those beneath the interface. With an assumption that the surface renewal period should be equal to the typical time scale of the quasi-streamwise vortex, the gas transfer rate was well predicted. The results indicate that it is the quasi-streamwise vortex scaled by the shear units that governs the mass transfer across a shear-driven air-water interface.

References

1. P. Lombardi, V. De Angelis and S. Banerjee. Direct Numerical Simulation of Near-Interface Turbulence in Coupled Gas-Liquid Flow. *Phys. Fluids*, 8-6: 1643-1665, 1996.
2. R. Nagaosa and R. A. Handler. Statistical Analysis of Coherent Vortices near a Free Surface in a Fully Developed Turbulence. *Phys. Fluids*, 15-2: 375-394, 2003.
3. V. De Angelis and S. Banerjee. Heat and Mass Transfer Mechanism at Wavy Gas-Liquid Interface. In *1st. Int. Symp. TSFP*, pp. 1249-1254, 1999.
4. D. V. Papavassiliou and T. J. Hanratty. The Use of Lagrangian Methods to Describe Turbulent Transport of Heat From a Wall. *Industrial Eng. Chem. Res.*, 34: 3359-3367, 1995.
5. A. Mitsuishi, Y. Hasegawa and N. Kasagi. Large Eddy Simulation of Mass Transfer across an Air-Water Interface at High Schmidt Numbers. In *6th. ASME/JSME Thermal Engineering Joint Conference*, TED-AJ03-231, 2003.
6. Y. Na and T. J. Hanratty. Limiting Behavior of Turbulent Scalar Transport Close to a Wall. *Int. J. Heat Mass Flow*, 43: 1749-1758, 2000.
7. T. J. Hanratty. Effect of Gas Flow on Physical Absorption. In *Air-Water Gas Transfer*, pp. 10-33, Amer Society of Civil Engineers Publ., 1991.
8. I. Calmet and J. Magnaudet. High-Schmidt Number Mass Transfer Through Gas-Liquid Interfaces. *Int. J. Heat Fluid Flow*, 19: 522-532, 1998.